
CERTIFICATE

It is certified that the work contained in the thesis titled ***“Corrosion and Low Cycle Fatigue Behaviour of Surface Modified Ti-13Nb-13Zr Alloy”*** by ***“Pramod Kumar”*** has been carried out under our supervision and this work has not been submitted elsewhere for a degree.

It is further certified that the student has fulfilled all the requirements of Comprehensive, Candidacy and SOTA for the award of Ph.D. degree.



Dr. Kausik Chattopadhyay
(Supervisor)

Department of Metallurgical Engineering
Indian Institute of Technology
(Banaras Hindu University)
Varanasi-221005, India



Dr. G. S. Mahobia
(Co-Supervisor)

Department of Metallurgical Engineering
Indian Institute of Technology
(Banaras Hindu University)
Varanasi-221005, India

DECLARATION BY THE CANDIDATE

I, "**Pramod Kumar**", certify that the work embodied in this thesis is my own bonafide work and carried out by me under the supervision of "**Dr. Kausik Chattopadhyay**" and "**Dr. G. S. Mahobia**" from "**July 2016**" to "**April 2022**", at the "**Department of Metallurgical Engineering**", Indian Institute of Technology (BHU), Varanasi. The matter embodied in this thesis has not been submitted for the award of any other degree/diploma. I declare that I have faithfully acknowledged and given credits to the research workers wherever their works have been cited in my work in this thesis. I further declare that I have not willfully copied any other's work, paragraphs, text, data, results, *etc.*, reported in journals, books, magazines, reports dissertations, theses, *etc.*, or available at websites and have not included them in this thesis and have not cited as my own work.

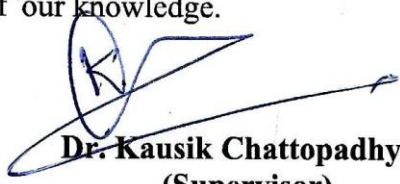


Date: 21-04-2022

Pramod Kumar

CERTIFICATE BY THE SUPERVISORS

It is certified that the above statement made by the student is correct to the best of our knowledge.



Dr. Kausik Chattopadhyay
(Supervisor)

Department of Metallurgical Engineering
Indian Institute of Technology
(Banaras Hindu University)
Varanasi-221005, India



Dr. G. S. Mahobia
(Co-Supervisor)

Department of Metallurgical Engineering
Indian Institute of Technology
(Banaras Hindu University)
Varanasi-221005, India



Dr. Sunil Mohan
(Professor and Head)

Department of Metallurgical Engineering
Indian Institute of Technology
(Banaras Hindu University)
Varanasi-221005, India
विभागाध्यक्ष/HEAD

धातुकीय अभियांत्रिकी विभाग
Department of Metallurgical Engg.
भारतीय प्रौद्योगिकी संस्थान (काशी हिन्दू विश्वविद्यालय)
Indian Institute of Technology (Banaras Hindu University)
वाराणसी-221005/Varanasi-221005

COPYRIGHT TRANSFER CERTIFICATE

Title of the Thesis:

“Corrosion and Low Cycle Fatigue Behaviour of Surface Modified Ti-13Nb-13Zr Alloy”

Name of the Student: Mr. Pramod Kumar

COPYRIGHT TRANSFER

The undersigned hereby assigns to the Indian Institute of Technology (Banaras Hindu University) Varanasi all rights under copyright that may exist in and for the above thesis submitted for the award of the "*Ph.D. Degree*".

Date: 21-04-2022


Pramod Kumar

Note: However, the author may reproduce or authorize others to reproduce material extracted verbatim from the thesis or derivative of the thesis for author's personal use provided that the source and the Institute's copyright notice are indicated.

Dedicated to
My Family

ACKNOWLEDGMENTS

I take this opportunity to express my sincere thanks and gratitude to my supervisors, Dr. Kausik Chattopadhyay and Dr. G. S. Mahobia for their consistent help, encouragement and valuable discussions during the entire period of my research work. Besides my supervisors, I would like to express my deepest sense of gratitude to Prof. Vakil Singh for continuous help and inspiration throughout my research. This thesis would not have been completed without their involvement and efforts. Because of their motivation I pursued my research problem. I consider myself extremely fortunate to have supervisors that genuinely cared about my work and responded to my queries timely.

I am highly thankful to Prof. Sunil Mohan, Head of the Department and former Heads, Prof. N. K. Mukhopadhyay and Prof. R.K. Mandal for providing all the research facilities to successfully complete my research in the Department. Besides my supervisors I sincerely thank RPEC committee members: Professor N. C. Santhi Srinivas, Department of Metallurgical Engineering and Dr. M. Z. Khan Yusufzai, Department of Mechanical Engineering, for their insightful comments and encouragement. My sincere thanks also go to Dr. R. Manna, Dr. B. Mukherjee and other faculty members of the Department of Metallurgical Engineering, IIT(BHU), for their cooperation in testing and support during thesis work.

I am also thankful to Prof. I. Samajdar, Professor, IIT Bombay, for residual stress measurements. My sincere thanks to Prof. S.R. Singh, Guest Faculty, School of Materials Science and Technology, IIT(BHU) for important and valuable suggestions in my research work. My special thanks to Dr. D. D. N. Singh, Ex-Scientist, NML Jamshedpur; Dr. Sumantra Mandal, Associate Professor, IIT Kharagpur; Dr. J. K. Singh, Research Professor, Hanyang; and Dr. Sumanta Kumar Pradhan for giving necessary suggestions

for corrosion studies. I would also like to thank Dr. Sanjeev Kumar Mahto, Associate Professor, School of Biomedical Engineering, IIT(BHU) for helping in study related to biocompatibility.

My thanks to all my seniors Dr. Sanjeev Rana, Dr. Preeti Verma, Dr. Vaibhav Pandey, Dr. Rupendra Singh Rajpurohit, Dr. Vikas Shivam, Dr. Raj Bahadur Singh, Dr. Manish Kishore Singh, Dr. Vivek Pandey, Dr. Ch. V. Rao, Dr. Yagnesh Shadangi, Dr. Asnit Gangwar, Dr. Chandra Shekhar Kumar and Dr. Neeraj Pandey for their needful help. I am also thankful to my colleagues Prerna, Sandeep, Jaydeep, Neelima, Shravan, Avnish, Aman, Subham, Debabrata, Roopchand, for making joyful and memorable life and being with my moments of happiness and troubles at IIT (BHU), Varanasi. I am also thankful to all my juniors from M. Tech and Ph. D. of our group from 2016 to 2022 for their support during my research work.

I am also thankful to all the Lab and workshop staff specially, Shri Sushil Ji, Mr. Kamlesh Ji, Mr. Anjani Ji, Mr. Minz Ji, Mr. Balwant Ji, Mr. Mangal Ji, Mr. Deepak Ji and Mr. Rajnarayan Ji for helping in preparation of fatigue and tensile samples. I would like to thank also Shri Lalit Kumar Singh, Shri Ashok Kumar Ji for helping in scanning and transmission electron microscopy. I would also like to extend my heartiest thanks to Prof. Rajiv Prakash (Prof. In-charge, CIFIC) and Mr. Girish Sahu, Mr. Vinay and Mr. Nirmal Mallick for needful help in SEM, TEM and other research facilities. My thanks to Patel Ji, Sushil Ji, Dubey Ji, Rana Ji, and all the other office and lab staff of the department.

I would also like to acknowledge the Ministry of Human Resource and Development, Government of India for providing teaching assistantship during the entire period of my Ph.D. Last, but not the least, I would like to express my deepest

gratitude to my parents Sri. Saudan Singh and Smt. Sheela Singh for their unconditional support and encouragement to pursue my interest. I would like to express my love and blessings to my sisters, Priyanka Shakya and Sunaina Shakya, for keeping me happy always with their interaction.

I also wish to thank all my friends and the persons whose names have not been mentioned on this piece of paper for extending their cooperation directly or indirectly.



Pramod Kumar

Table of Contents

	<u>Page No.</u>
List of Figures	xix
List of Tables	xxvii
Abbreviations	xxix
Symbols	xxxiii
PREFACE	xxxvii
Chapter 1	1
Introduction And Literature Review	1
1.1 Biomaterials.....	1
1.2 Titanium and Titanium Alloys	2
1.3 Biomedical Applications of Titanium Alloys.....	7
1.4 Impact of Microstructural Modification on Mechanical Properties	10
1.5 Importance of Elastic Modulus	20
1.6 Effect of USSP on Microstructure.....	23
1.7 Corrosion Behaviour	24
1.8 Fatigue Behaviour	28
1.9 Osseointegration	31
1.10 Scope of The Present Investigation	35
1.11 Objectives of the Present Investigation	36
Chapter 2	37
Material and Experimental Details	37

2.1 Introduction.....	37
2.2 Material	37
2.3 Ultrasonic Shot Peening Treatment	38
2.4 Microstructural Characterization	39
2.5 Mechanical Properties.....	41
2.6 Electrochemical Corrosion Measurements	44
2.7 Bioactivity Tests	46
Chapter 3	49
Elastic Modulus and Tensile Behaviour	49
3.1 Introduction.....	49
3.2 Microstructural Characterization	49
3.3 Microhardness.....	53
3.4 Elastic Modulus	53
3.5 Tensile Properties.....	54
3.6 Discussion.....	57
3.7 Conclusions.....	61
Chapter 4	63
Microstructural Characterization and Microhardness variation after USSP treatment.....	63
4.1 Introduction.....	63
4.2 Microstructural Characterization	63
4.3 Surface Roughness.....	69

4.4 Microhardness	71
4.5 Residual Stress.....	73
4.6 Discussion.....	74
4.7 Conclusions	78
Chapter 5.....	81
Effect of USSP on Corrosion Resistance	81
5.1 Introduction	81
5.2 USSP Treatment	81
5.3 Corrosion Properties.....	82
5.4 Weight Loss in Static Immersion tests	89
5.5 Chemical Analysis by XPS	93
5.6 Discussion.....	96
5.7 Conclusions	104
Chapter 6.....	105
Effect of USSP on Low Cycle Fatigue Behaviour.....	105
6.1 Introduction	105
6.2 Microstructure	106
6.3 Roughness.....	107
6.4 Microhardness	108
6.5 Residual Stress.....	109
6.6 Low Cycle Fatigue Behaviour.....	110
6.7 Discussion.....	120

6.8 Conclusions.....	126
Chapter 7	127
Influence of USSP and Subsequent Stress Relieving on Biocompatibility and Cell Response.....	127
7.1 Introduction.....	127
7.2 Sample Preparation	128
7.3 Osseointegration	128
7.4 Wettability test.....	130
7.5 Cell Culture.....	132
7.6 MTT Assay	135
7.7 Discussion.....	136
7.8 Conclusions.....	140
Chapter 8	141
Summary and Suggestions for Future Work	141
8.1 Introduction.....	141
8.2 Summary	141
8.3 Suggestions for Future Work.....	145
Bibliography	146
List of Publications	173
International Conferences.....	173

List of Figures

<u>Figure No.</u>	<u>Figure Caption</u>	<u>Page No.</u>
Figure 1.1 (a)	The hcp (alpha) and bcc (beta) structure of titanium.	
(b)	Categories of titanium phase diagrams formed with different alloying additions.	3
Figure 1.2	Key microstructural phases observed in various types of microstructures in a wide range of titanium alloys.	5
Figure 1.3	Biomedical applications of titanium alloys.	8
Figure 1.4	Laser shock peening process.....	16
Figure 1.5	Shot peening process.	17
Figure 1.6	Schematic of (a) ultrasonic shot peening instrument, (b) chamber assembly, and (c) principle of ultrasonic shot peening.	18
Figure 1.7	Stress shielding phenomenon.....	20
Figure 1.8	Elastic modulus of currently used biomedical alloys.	21
Figure 1.9	Bright field TEM micrographs with related SAED patterns taken at depths of (a) 5 μm and (b) 20 μm from the surface of the alloy Ti–6Al–4V following USSP with 3 mm balls.	23
Figure 1.10 (a)	TEM micrograph and, the corresponding (b) SAED pattern of Ti-Nb-Zr-Fe alloy after 60 minutes of SMAT treatment by 8 mm steel shots.	24
Figure 1.11 (a)	Cyclic polarization curves of β solution treated specimens with different cooling conditions of Ti–13Nb–	

13Zr alloy in Ringer's solution; (b) Polarization curves of Ti-13Nb-13Zr and Ti-15Mo in aerated Ringer's solution.....	26
Figure 1.12 (a) Stress controlled fatigue (S-N) curve and, (b) Strain- controlled fatigue data of of Ti-7.5Mo, Ti-13Nb-13Zr, Cp-Ti, and Ti-6Al-4V alloy in their cast condition	29
Figure 1.13 Cell cultured on Cp-Ti samples (a) for three days, USSP treated for 30, 60, 90 and 120 seconds; followed by stress relieving, (b) for 1, 2 and 3 days, USSP treated for 45 minutes and annealed.....	33
Figure 2.1 Schematic representation of Ultrasonic shot peening set-up	38
Figure 2.2 Ultrasonic velocity gauge for elastic modulus measurement.....	41
Figure 2.3 Geometry of tensile test sample.	42
Figure 2.4 Geometry of LCF test sample.	43
Figure 2.5 Test samples suspended in Ringer's solution for static immersion test.....	45
Figure 3.1 Heat treatment outline for the alloy Ti-13Nb-13Zr.....	49
Figure 3.2 Optical microstructures of the Ti-13Nb-13Zr alloy in different conditions (a) AR, (b) 660WQ, (c) 900WQ and (d) 900SZQ. Magnified views are shown in the insets.....	50
Figure 3.3 XRD patterns of the Ti-13Nb-13Zr alloy in different conditions.....	51
Figure 3.4 Variation of microhardness in different conditions.....	53
Figure 3.5 Elastic modulus of Ti-13Nb-13Zr alloy in different conditions, measured by ultrasonic testing	54

Figure 3.6 Typical stress-strain curves of Ti-13Nb-13Zr alloy in different conditions.....	55
Figure 3.7 SEM fractographs of tensile tested samples with different conditions: (a) AR, (b) 660WQ, (c) 900WQ and (d) 900SZQ, showing dimple morphology	56
Figure 4.1 (a) Optical, (b) SEM, and (c) TEM micrographs of the Un- USSP (900WQ) sample.....	64
Figure 4.2 TEM micrographs of (a) of α' (hcp) and (c) β (bcc) phases, along with respective SAED patterns shown in (b) and (d)..	65
Figure 4.3 XRD profiles of the Un-USSP and USSP treated specimens (used for corrosion study).....	66
Figure 4.4 XRD profiles of the Un-USSP and USSP treated specimens (used for low cycle fatigue study).	66
Figure 4.5 Typical TEM micrographs with respective SAED patterns, of the different conditions: (a) Un-USSP showing twins and dislocations, (b) USSP30, (c) USSP60, and (d) USSP120.....	68
Figure 4.6 Variation of average surface roughness with duration of USSP.	70
Figure 4.7 SEM images of the (a) Un-USSP, (b) USSP30, (c) USSP60 and (d) USSP120 specimen showing surface cracks.....	71
Figure 4.8 Microhardness variation along the depth of the Un-USSP and USSP treated samples.....	72

Figure 4.9 SEM micrographs of the (a) USSP120, (b) USSP240, and (c) USSP360 samples, showing depth of modified layer on the longitudinal mid-section of the specimens.	72
Figure 4.10 Surface residual stress of the Un-USSP and USSP treated specimens.....	73
Figure 5.1 Potentiodynamic polarization curves of the Un-USSP and USSP treated samples.	83
Figure 5.2 Nyquist diagrams of the Un-USSP and USSP treated Ti- 13Nb-13Zr specimens.....	86
Figure 5.3 Equivalent circuit diagram for the fitting of EIS data.....	86
Figure 5.4 Bode diagrams (a) log-log plot of $ Z $ vs. freq. and (b) log- log plot of phase angle vs. freq., of Un-USSP and USSP treated specimens. The experimental data are shown by the symbols and the simulated data are shown as the solid lines.....	87
Figure 5.5 Weight change in the Un-USSP and USSP treated samples after static immersion in Ringer's solution, at room temperature.	90
Figure 5.6 Corrosion rate of the Un-USSP and USSP treated samples after 35 weeks of immersion in Ringer's solution.....	90
Figure 5.7 SEM images along with EDS of the (a) Un-USSP, (c) USSP30, (e) USSP60, and (g) USSP120 samples after 35 weeks of immersion in the Ringer's solution.	92
Figure 5.8 Typical XPS survey data of the USSP30 and Un-USSP specimens.....	93

Figure 5.9 High resolution XPS showing Ti 2p, Nb 3d, Zr 3d, Ca 2p, P 2p, and O 1s of the Ti-13Nb-13Zr alloy, in the USSP30 and Un-USSP condition.	94
Figure 5.10 Schematic illustration of the passive layer and associated compressive residual stress in different conditions (a) Un- USSP, (b) USSP30, and (c) USSP120 samples.....	95
Figure 6.1 XRD peaks of the Un-USSP, USSP240 and USSP240-SR samples.	106
Figure 6.2 Variation of hardness across the depth of Un-USSP, USSP240 and USSP240-SR samples.	108
Figure 6.3 Residual stress as a function of depth in USSP240 and USSP240-SR samples.	109
Figure 6.4 Cyclic stress response curves of (a) Un-USSP, (b) USSP240 and (c) USSP240-SR samples.....	111
Figure 6.5 Fatigue hysteresis loops for first cycles in the Un-USSP, USSP240 and USSP240-SR conditions.	112
Figure 6.6 Coffin-Manson plot for the Un-USSP, USSP240 and USSP240-SR samples.	113
Figure 6.7 Fatigue life cycles for the Un-USSP, USSP240 and USSP240-SR conditions, at different total strain amplitudes.	114
Figure 6.8 SEM micrographs showing fracture surface of Un-USSP, USSP240 treated and USSP-SR samples, at different total strain amplitudes.....	116

Figure 6.9 SEM micrographs showing fracture surface morphology of Un-USSP, USSP240 treated and USSP240-SR samples, at different total strain amplitudes.	117
Figure 6.10 TEM images of Un-USSP sample, fatigue tested at $\pm 0.70\%$ strain amplitude showing; (a) α' laths with twinned region identified by (b) double diffraction spots in SAED pattern.....	118
Figure 6.11 TEM images of USSP240 sample, fatigue tested at $\pm 0.70\%$ strain amplitude showing α' laths having (a) twin variants PT (primary twins) and ST (secondary twins) (b) enlarged view of red marked area and (c) corresponding SAED pattern along the $[1\bar{2}1\bar{3}]_{\alpha'}$ zone axis indicating cross twins identified as two twin variants of the $\{1\bar{1}01\}$ twinning system.....	118
Figure 6.12 TEM images of USSP240 sample fatigue tested at $\pm 0.70\%$ strain amplitude having α' laths with (a) dislocation tangles (b) SAED pattern along the $[1\bar{2}1\bar{3}]_{\alpha'}$ zone axis (c) twin-twin intersection.....	119
Figure 6.13 TEM images of USSP240-SR sample fatigue tested at $\pm 0.70\%$ strain amplitude having α' laths (a) twinned region (b) enlarged view along with (c) SAED pattern along the $[2\bar{4}2\bar{3}]_{\alpha'}$ zone axis.....	119
Figure 7.1 Contact angles formed by distilled water droplets, applied on the surface of the Un-USSP, USSP and USSP-SR samples.....	131

Figure 7.2 Cell culture images of on the various Un-USSP and USSP samples after 2 days of incubation. Blue color: nuclei staining; red color: actin cytoskeleton filaments staining.133

Figure 7.3 Cell culture images of on the various Un-USSP and USSP samples after 4 days of incubation. Blue color: nuclei staining; red color: actin cytoskeleton filaments staining.134

Figure 7.4 Cell culture images of on the various USSP-SR samples after 2 days of incubation. Blue color: nuclei staining; red color: actin cytoskeleton filaments staining.134

Figure 7.5 Cell culture images of on the various USSP-SR samples after 4 days of incubation. Blue color: nuclei staining; red color: actin cytoskeleton filaments staining.135

Figure 7.6 Histograms showing relative cell viability measured for the Un-USSP, USSP and USSP-SR conditions. The absorbance of the control for the second day culture was used as a reference for all the samples in this experiment.136

List of Tables

<u>Table No.</u>	<u>Table Caption</u>	<u>Page No.</u>
Table 1.1	Some α , $\alpha+\beta$, β titanium alloys and their tensile properties.....	4
Table 1.2	Tensile properties of main metallic biomaterials in annealed condition.....	10
Table 1.3	The basic difference between SP and USSP	19
Table 2.1	Chemical composition of the Ti-13Nb-13Zr alloy (wt%).....	37
Table 2.2	Processing parameters of USSP.....	38
Table 2.3	Test matrix for LCF tests.	44
Table 3.1	Different phases and their volume fractions in different conditions.	52
Table 3.2	Tensile properties* in the as-received and different heat- treated conditions.	55
Table 3.3	Effect of the different processes and heat treatments on modulus and other tensile properties* of the alloy Ti- 13Nb-13Zr, reported earlier	60
Table 4.1	Designations of the USSP treated specimens.....	64
Table 4.2	Calculated crystallite size and mean micro-strain of the USSP treated specimens.....	67
Table 4.3	Surface roughness* of the Un-USSP and USSP treated specimens.	70
Table 5.1	Designations of the USSP treated specimens.....	82

Table 5.2 Electrochemical parameters of the Un-USSP and USSP treated specimens extracted from polarization plots fitted in the Tafel regions.	84
Table 5.3 EIS data simulation for the Un-USSP and USSP treated specimens.....	87
Table 5.4 Surface composition from XPS spectra of Un-USSP and USSP30 sample.....	94
Table 6.1 Surface roughness* of the Un-USSP, USSP240 and USSP240-SR treated specimens.	107
Table 6.2 Fatigue life of the specimens USSP treated for different durations at $\Delta\epsilon_t/2=\pm 0.70\%$	110
Table 6.3 LCF parameters calculated from Coffin-Manson plot for the Un-USSP, USSP240 and USSP240-SR conditions.....	113
Table 6.4 Low cycle fatigue data in Un-USSP, USSP240 and USSP240-SR conditions of samples at different total strain amplitudes.	114
Table 7.1 Wettability of the Un-USSP, USSP and USSP-SR samples.	130

Abbreviations

AC	Air Cooled
AISI	American Iron and Steel Institute
ALP	Alkaline Phosphatase
AR	As Received
ASTM	American Society for Testing and Materials
BCC	Body Centred Cubic
CPE	Constant Phase Element
Cp-Ti	Commercially Pure Titanium
CR	Corrosion Rate
CRSS	Critically Resolved Shear Stress
DT	Damage Tolerance
EBS	Electron Back Scattered Diffraction
EDS/EDX	Energy Dispersive X-ray Spectroscopy
EIS	Electrochemical Impedance Spectroscopy
ELI	Extra Low Interstitials
FC	Furnace Cooled
FCC	Face Centred Cubic
FCP	Fatigue Crack Propagation
FESEM	Field Emission Scanning Electron Microscope
GNS	Gradient Nano Structure
HCF	High Cycle Fatigue
HCP	Hexagonal Closed Packing
HPT	High Pressure Torsion

HRTEM	H igh R esolution T ransmission E lectron M icroscope
LCF	L ow C ycle F atigue
MB	M icro B and
MTT	3-(4,5-Di- M ethyl- T hiazol-2-yl)-2,5-Diphenyl T etrazolium bromide
OCP	O pen C ircuit P otential
PBS	P hosphate B uffered S aline
PD	P otential D ynamic
SAED	S electd A rea E lectron D iffraction
SC	S econdary C racks
SEM	S canning E lectron M icroscope
SFE	S tacking F ault E nergy
SMAT	S urface M echanical A ttriton T reatment
SPD	S evere P lastic D eformation
SR	S tress R elieving
SS	S tainless S teel
SSP	S evere S hot P eening
ST	S olution T reatment
SZQ	S ub Z ero Q uenced
TEM	T ransmission E lectron M icroscopy
UN-USSP	U n- U ltrasonic S hot P eened
USSP	U ltrasonic S hot P eening
USSP-SR	U ltrasonic S hot P eened- S tress R elieved
WQ	W ater Q uenced
XPS	X - R ay P hotoelectron S pectroscopy
XRD	X - R ay D iffraction

Z_{img} Impedance **I**maginary **C**omponent

Z_{real} Impedance **R**ead **C**omponent

Symbols

°C	Degree Centigrade
µm	Micrometre
nm	Nanometre
α	Alpha
β	Beta
θ	Theta
ω	Omega
wt%	Weight Percent
kHz	Kilo Hertz
mHz	Milli Hertz
mg	Milligram
mm	Millimetre
ml	Millilitre
t	Effective size of crystallite
A	Area
a	Lattice Parameter
B	Line Broadening
D	Average Crystallite Size
cm	Centimetre
s	Second
K	Constant
W	Mass Loss(mg)

kN	kilo Newton
kV	kilo Volt
>	Greater than
<	Less than
λ	Wavelength
ε	Root mean square of micro-strain
$\Delta\varepsilon_t/2$	Total strain amplitude
$\Delta\varepsilon_p/2$	Plastic strain amplitude
$\Delta\varepsilon_e/2$	Elastic strain amplitude
MPa	Mega Pascal
R_a	Average Surface Roughness
R_q	Root mean square (RMS) roughness
R_z	Average maximum height of the profile
H_v	Vickers hardness
ν	Poisson's Ratio
$2N_f$	Number of reversals to failure
ε'_f	Fatigue ductility coefficient
I_{corr}	Corrosion current
E_{corr}	Corrosion potential
β_a	Anodic Tafel slope
β_c	Cathodic Tafel slope
d	density
V_T	Transverse Velocity
V_L	Longitudinal Velocity

E	Elastic Modulus
μA	Microampere
Q	constant (87600)

PREFACE

During the last decade, there has been extensive use of titanium and its alloys for biomedical applications. Titanium and its alloys have modulus of elasticity lower than other metallic biomaterials such as stainless steels and Co-Cr alloys. In general, elastic moduli of β -type titanium alloys is much lower than those of α and $(\alpha + \beta)$ type titanium alloys. Among titanium alloys, developed for aerospace applications, Ti-6Al-4V was the first titanium alloy to be used as biomedical implants. However, some health issues have been reported to be associated with the release of vanadium and aluminium ions from Ti-6Al-4V alloy. Another disadvantage is the mismatch of modulus of elasticity of Ti-6Al-4V (~120 GPa) with that of human bone (~30 GPa), that creates stress shielding effect between the implant and human bone, causing excessive bone resorption and loss of bone. Consequently, non-toxicity of implant and its low elastic modulus are the two crucial requirements for a suitable titanium bio-implant. Much of the research of biomaterials has been focused on reducing elastic modulus of materials for biomedical applications. Alloying of titanium with non-allergic beta stabilizing elements such as Nb, Zr, Mo, Ta and Sn shows possibility of controlling modulus of elasticity through various heat treatments. Beta titanium alloys, in addition to low elastic modulus also possess adequate mechanical properties and wear resistance.

Titanium and its alloys are in much demand for bio-medical applications because of their good corrosion resistance, specific strength and biocompatibility. Improved corrosion resistance of such titanium alloys is due to formation of a stable passive oxide layer at the surface. The electrochemical and physicochemical properties of the passive oxide layer play a vital role in the process of osseointegration and biocompatibility of

titanium implants. Corrosion is one of the main challenges for ensuring stability and biocompatibility of metallic implants.

Both corrosion as well as fatigue failure in most of the materials occurs from the surface; therefore, through surface modification, the performance of metallic materials can be effectively improved. Several researchers have worked on improving lifetime of titanium implants through surface modification. In commercially pure titanium, a nanocrystalline layer was developed by ultrasonic shot peening (USSP) technique and was found to cause significant improvement in its fatigue life and surface hardness. Many researchers have found USSP a potential process for enhancing hardness, corrosion resistance and fatigue resistance through inducement of large amount of compressive residual stresses as well as grain refinement in the surface region of materials. This process can be controlled to produce rapid nanostructuring and gradient microstructure in short duration with high energy of impacts.

The present investigation deals with the influence of heat treatments on the microstructure, hardness, tensile behaviour and elastic modulus of the near- β Ti-13Nb-13Zr alloy. It also presents the effect of USSP treatment on surface microstructure modification, corrosion behaviour, low cycle fatigue and in-vitro biocompatibility of the alloy. This thesis comprises of eight chapters.

Chapter 1 presents brief introduction along with literature review on the properties and applications of the Ti-13Nb-13Zr alloy. It also presents the details of grain refinement processes in metals/alloys. USSP improves both fatigue and corrosion resistance of titanium alloys. The objectives of the present investigation are listed at the end of this chapter.

Chapter 2 presents details of the material, Ti-13Nb-13Zr alloy, and the procedure of its characterization before and after heat treatment. The alloy Ti-13Nb-13Zr was procured from Baoji Kedipu Shaanxi, China, as rod of 30 mm diameter. It was cut into pieces of 110 mm length and pieces were longitudinally sectioned into two halves, to be machined into cylindrical shape of 12 mm diameter, for machining of cylindrical fatigue test samples. The cylindrical blanks were subjected to two different solution treatment temperatures and quenched at different temperatures. Three different heat treatments were given. Two samples were solution treated at 900°C (above β transus~735°C) for 1 hour, one was quenched in water at room temperature (25°C) and the other in alcohol maintained at sub-zero temperature (-30°C), and these are designated as 900WQ and 900SZQ, respectively. The third sample was solution treated at 660°C and quenched in water and designated as 660WQ. The microstructure is characterized before and after ultrasonic shot peening (USSP) treatment. The procedures of characterization like optical microscopy, scanning electron microscopy, transmission electron microscopy, electron probe micro-analysis and X-ray diffraction are described. The procedures of the measurement of elastic modulus of the heat-treated samples, evaluation of surface roughness and microhardness are also described. Test procedures for electrochemical corrosion by potentiodynamic polarization, electrochemical impedance spectroscopy and static immersion tests inside Ringer's solution are presented. The procedure of conducting low cycle fatigue tests is described. The methods used for biocompatibility study through cell proliferation and cell adhesion tests are described.

Chapter 3 presents the effect of three different heat treatments on modulus and tensile properties of the Ti-13Nb-13Zr alloy. The alloy was subjected to two different solution treatment temperatures and quenched at different temperatures. Elastic modulus was decreased with increase in the cooling rate, following the solution treatment. The

samples solution treated at 900° C and quenched at sub-zero temperature, contained α'' martensite along with α' and β phases and the elastic modulus was lowered. Among all the heat-treated samples, the one solution treated at 900°C and quenched in water, exhibited lowest elastic modulus of 60 GPa and adequate tensile properties for applications as bioimplants.

Chapter 4 presents the effect of USSP treatment on the microstructure modification, surface roughness, microhardness and residual stress of the material. The heat-treated alloy with low elastic modulus, and optimum mechanical properties was selected and given USSP treatments for different durations of 15 to 360 seconds. Microstructural changes were examined using XRD, SEM and TEM. The average surface roughness was found to increase with increase in the USSP duration. Microhardness was observed to be highest in the surface region, and gradually decrease towards the substrate. Microhardness and also the depth of modification increased with duration of USSP treatment. No phase transformation was observed due to USSP treatment, as confirmed through XRD. Nano size grains of 21, 13 and 12 nm were observed in the surface region of the alloy; after 120, 240 and 360 seconds of USSP duration.

Chapter 5 describes the effect of the USSP on corrosion behaviour of the Ti-13Nb-13Zr alloy in Ringer's solution by electrochemical impedance spectroscopy, potentiodynamic polarization and static immersion tests. The electrochemical study revealed reduction in corrosion of the USSP treated samples. Grain refinement and surface roughness were the two opposing factors controlling the corrosion behaviour. Besides refined grain size and the presence of surface compressive residual stresses, the appropriate USSP duration produced optimal corrosion resistance. There was maximum passivation from the 30 s of USSP treatment, and it decreased with an increase in the

USSP duration. The improvement in corrosion resistance from the USSP was due to grain refinement and the associated compressive residual stresses in the surface region.

Chapter 6 describes the influence of USSP as well that of stress-relieving 400°C for 1 hour (USSP-SR), on low cycle fatigue life of the Ti-13Nb-13Zr alloy, at room temperature. The results are discussed in terms of surface nano structuring and the compressive residual stress associated with the affected region. The gauge section of fatigue samples was subjected to USSP treatment uniformly, for different durations, by rotating the sample to ensure uniform peening along circumference of the gauge section for 4 minutes duration. Low cycle fatigue tests were conducted for non-USSP, USSP, and USSP-SR conditions under fully reversible ($R = -1$) axial loading, with triangular waveform, at total strain amplitudes of $\pm 0.55\%$, $\pm 0.60\%$, $\pm 0.70\%$, $\pm 0.80\%$, and $\pm 0.90\%$, at a fixed strain rate of 0.005 s^{-1} . The microstructure and fracture morphology of the fatigue tested specimens are analyzed using scanning electron microscope. Low cycle Fatigue (LCF) tests were first conducted at $\pm 0.70\%$ total strain amplitude for the samples USSP treated for 120, 240 and 360 s of duration to find out the best fatigue life with respect to the peening duration. LCF life was increased considerably for all the specimens subjected to USSP treatment of 120-360 seconds but the optimum enhancement was seen in the specimen USSP treated for 240 s, in which fatigue life was enhanced nearly three times. Fatigue crack initiation in the un-treated and USSP-SR samples was found from the surface, whereas it was from subsurface in the USSP treated samples.

Chapter 7 deals with the in-vitro biocompatibility study of the alloy in non-USSP, USSP and USSP-SR conditions using cell proliferation and cell adhesion tests. Disc-shaped samples of 3 mm diameter and 2 mm thickness were prepared from the as heat-treated Ti-13Nb-13Zr alloy, with optimal elastic modulus and mechanical properties. MTT (4,5-di-methyl-thiazol-2-yl-2,5-diphenyl tetrazolium bromide) assay

was performed for checking cell proliferation/cell viability using a standard microplate absorbance reader. The increase in cellular activity increases the formation of formazan crystal, thereby increasing the absorbance value, which is directly proportional to the active cells. MG63 cells (10^4 cells/well) were seeded on the surface and after 48 h of incubation, relative cell viability was measured. A significant increase in cell proliferation is observed with increase in USSP duration. After 48 hours of incubation, there is about 1.6 times increase in cell viability of the MG-63 cells after 120 s USSP treatment, due to increased roughness and formation of nano-structures, with high positive potential. Improved cell viability in USSP-SR samples can be attributed to the increased osteoblast anchorage due to combined effect of roughness and formation of biocompatible oxide layer on the surface via stress-relieving treatment. A good amount of cell coverage can also be observed in fluorescence microscopy images of the USSP and USSP-SR samples compared to Un-USSP samples. It was observed from this study that USSP treatment on alloy surface significantly changed the surface architecture to nano level, which led to enhanced Osteoblast cell adhesion and proliferation.

Chapter 8 presents major conclusions drawn from the present investigation along with suggestions for the future work.